# Formation Pathways of Metal Organic Frameworks Proceeding Through Partial Dissolution of the Metastable Phase

Samantha L. Anderson,[a] Andrzej Gładysiak,[a] Peter G. Boyd,[a] Christopher P. Ireland,[a] Pascal Miéville,[b] Davide Tiana,[a] Bess Vlaisavljevich,[c] Pascal Schouwink,[b] Wouter van Beek,[d] Kevin J. Gagnon,[e] Berend Smit[a,c] and Kyriakos C. Stylianou[a]*

a) Laboratory for Molecular Simulations (LSMO), Institut des Sciences et Ingénierie Chimiques (ISIC), École Polytechnique Fédérale de Lausanne (EPFL Valais Wallis), Rue de l'Industrie 17, CH-1951 Sion, Switzerland.
b) Institut des Sciences et Ingénierie Chimiques (ISIC), École Polytechnique Fédérale de Lausanne (EPFL), CH-1015, Lausanne, Switzerland.
c) Department of Chemical and Biomolecular Engineering, University of California, Berkeley 94720, USA
d) Swiss-Norwegian Beamlines at ESRF, BP 220, Grenoble, France
e) Advanced Light Source, Lawrence Berkeley National Laboratory, Berkeley, California, 94720, USA

## Abstract

Understanding how crystalline materials are assembled is important for the rational design of metal organic frameworks (MOFs), through streamlining their synthesis and controlling their properties for targeted applications. Herein, we report for the first time the construction of two 3-dimensional Tb(III) based MOFs; a metastable MOF acting as an intermediate phase, that partially dissolves and transforms into a chemically and thermodynamically stable MOF. This chemical transformation occurs solely in a *N,N*-dimethylformamide/water solvent mixture, and is triggered when additional energy is provided to the reaction. *In situ* studies reveal the partial dissolution of the metastable phase after which the MOF components are reassembled into the thermodynamically stable phase. The marked difference in thermal and chemical stability between the kinetically and thermodynamically controlled phases is contrasted by their identical chemical building unit composition.

## Introduction

From the 19th century to the present day, researchers have demonstrated that chemical compounds can form two or more solid phases,[1] such as in calcium carbonate minerals,[2] and $TiO_2$.[3] These polymorphs or metastable phases can be formed through the addition of additives, or changes in the reaction conditions,[4] and for many practical applications it is important to determine the correct conditions for the formation of the desired phase. However, understanding the underlying mechanism that guides the formation of these phases is limited, thereby restricting access to materials that otherwise may be difficult to form through traditional methods.[4c] Metal organic frameworks (MOFs) are crystalline porous materials composed of metal ions or clusters and organic ligands.[5] The self-assembly of the components in MOFs is a dynamical non-equilibrium process, evolving from an initially disordered state, towards an ordered stable state by the completion of the reaction.[6] This process can proceed through various pathways, where structures can either be described as under kinetic or thermodynamic control.[1a-c, 6-7] Revealing the pathways in the synthesis of MOFs remains a challenge, since there are limited experimental methods available that can provide high quality *in-situ* data. [4a, 4b, 8] We are only beginning to reveal the dynamic nature of these reactions, as recent studies have challenged the conventional view that once the MOF crystal is formed it remains stable in solution.[9,10] For example, it was demonstrated that Zn(II) ions in MOF-5 undergo a coordination/decoordination phenomenon in which the DMF solvent, the metal center and the ligand have a dynamic relationship revealing that the assumed rigid coordination motif is in reality more dynamic.[4c] Through the understanding of this behaviour, methods can be developed to afford previously unavailable MOF analogues, such as Co(II) substituted MOF-5,[4c] or gain fundamental insights on the formation of kinetic and thermodynamic MOF products and their influence on the formation of the final framework.[10c]

A key issue hindering the fundamental insights into the formation of MOFs is the lack of model systems in which different frameworks composed of the same chemical components can be systematically studied. This work presents two 3-dimensional Tb(III) based MOFs utilizing a DHBDC (DHBDC = 2,5-dihydroxybenzene-1,4-dicarboxylate) ligand; **SION-1** and **SION-2** (SION refers to MOFs synthesized at the EPFL Valais in Sion, Switzerland). Uniquely, this systematic study reveals tuneable conditions favouring the formation of one phase or the other, and *in-situ* $^1$H NMR and powder X-ray diffraction studies on how **SION-2** transforms to **SION-1**. This tunability arises from the addition of more energy allowing the kinetic and metastable **SION-2** to partially dissolve and undergo a structural rearrangement into the thermodynamically stable **SION-1**.

## Structural Description and Stability of SION-1 and SION-2

### Structural Analysis of SION-1 and SION-2 Single Crystals

The reaction of $Tb(NO_3)_3 \cdot 6H_2O$ with $H_2DHDBC$ in DMF:$H_2O$ solvent mixture at 120 $^oC$ for 24 hours yielded gold coloured crystals of **SION-2** (see SI, section S1)**. SION-2** crystals were analysed using single crystal X-ray diffraction (SCXRD, SI Section 2.1) and its formula is based on $[Tb_2(DHBDC)_3(DMF)_4] \cdot 2DMF$ (general formula $M_2L_3$, where M:Tb(III) and L:DHBDC). **SION-2** crystallizes in the triclinic space group $P\bar{1}$ and is composed of a binuclear $Tb_2(COO)_6$ cluster interconnected by three distinct DHBDC ligands (Fig. 1a). Each of these ligands possess a centre of symmetry which is retained within the crystal structure. The $Tb_2$-clusters are centrosymmetrical as well, and each 8-coordinated Tb(III) displays a square antiprismatic geometry (Fig. 1b), which is completed via coordination of two fully ordered DMF molecules, two carboxylate O-atoms from a $\eta^2$ chelating DHBDC ligand, and the remaining four carboxylate O-atoms from two symmetrically distinct DHBDC with $\eta^1$:$\eta^1$ bridging modes (Fig. 1c). Here, the hydroxyl groups of the DHBDC ligands do not participate in metal binding. **SION-2** possesses rectangular channels running along the crystallographic direction of [100] which are filled with coordinated to Tb(III) and guest DMF molecules (Fig. 1d), the latter being disordered over two sites with unequal occupancies. We note that **SION-2** is isomorphous to the structures of $[Ln_2(DHBDC)_3(DMF)_4] \cdot 2DMF$ (Ln = La, Ce, Pr, Nd, Sm, Gd, Er) reported previously.[11] Topological analysis of **SION-2** using the TOPOS4.0 software package designates this material as the ***xah*** topology, using the three-letter notation of O'Keeffe (Fig. S6).[12]

The reaction of $Tb(NO_3)_3 \cdot 6H_2O$ with $H_2DHDBC$ in DMF:$H_2O$ solvent mixture at 120 $^oC$ for 72 hours gave rise to red single crystals of **SION-1** (see SI, section S1). **SION-1** has a formula of $[Tb_2(DHBDC)(DOBDC)(DMF)_2]$, (where: DOBDC = 2,5-dioxidobenzene-1,4-dicarboxylate), or a general formula of $M_2L_2$, and possesses a higher monoclinic symmetry (space group $P2_1/n$, SI Setion S2.2). The DHBDC and DOBDC ligands are symmetrically independent and their centres of gravity sit on crystallographic inversion centres. The main building unit of **SION-1** consists of $2_1$- symmetrical chains of alternating Tb(III) and O atoms that are running along the [010] direction (Fig.2a). Visually, the structure appears to resemble a ladder, and within these ladder-like arrays, the coordination number of each Tb(III) is 8 with a distorted dodecahedron geometry, where only one out of eight coordination sites is occupied by DMF molecules (Fig. 2b), which are disordered over two sites with unequal occupancies. The DHBDC ligands with protonated hydroxyl groups bind to Tb(III) in a similar coordination mode with the $\eta^1$:$\eta^1$ bridging ligands in **SION-2**, demonstrating a similar partial disorder over the two pendant hydroxyl groups (Fig. 2c-d). However, the fully deprotonated DOBDC has a $\eta^1$:$\eta^2$:$\eta^2$ bridging mode and binds to Tb(III) in a similar way as observed in MOF-74.[13] This highly-connected coordination mode allows for the formation of 2-dimensional puckered sheets consisting of Tb(III) and O-atoms (Fig. 2e) which are interlinked by the DHBDC to form a 3-dimensional structure with 1-dimensional channels running along [010] (Fig. 2f).

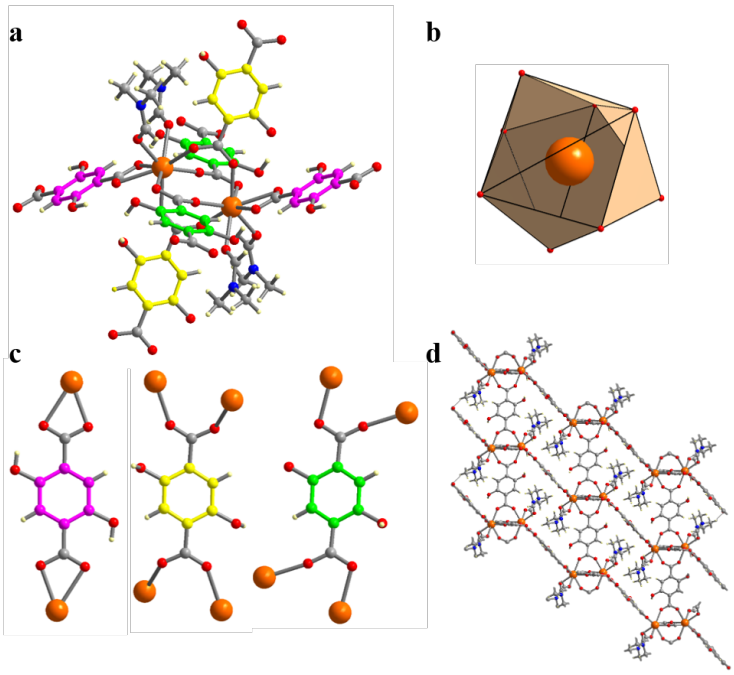


**Fig.1. SION-2 a.** $Tb_2$-cluster **b.** antiprismatic coordination geometry of Tb(III), **c.** coordination modes of the three distinct ligands with $\eta^2$ chelating (purple) and $\eta^1$:$\eta^1$ bridging (yellow and green) modes and **d.** the packing along the crystallographic [100] direction with coordinated DMF molecules occupying the accessible void space. Atom colours: orange, Tb; red, O; blue, N; grey, C; pale yellow, H.

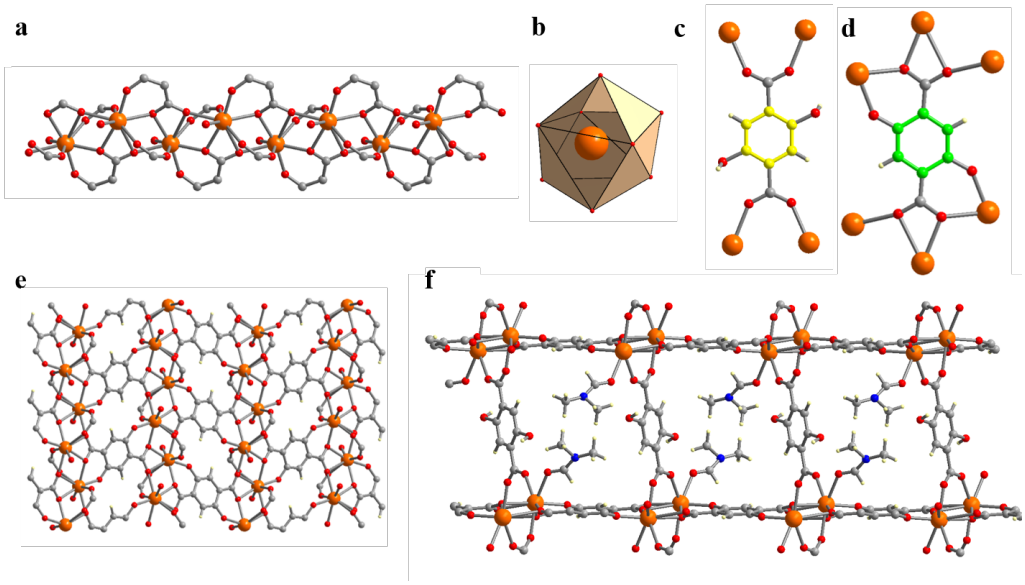


**Fig. 2. SION-1 a.** 1-dimensional Tb-O chains running along the crystallographic [010] direction, **b.** distorted dodecahedron geometry of Tb(III) **c.** and **d.** coordination schemes of DHBDC and DOBDC ligands in **SION-1** ($\eta^1$:$\eta^1$ bridging – yellow and $\eta^1$:$\eta^2$:$\eta^2$ bridging – green, respectively), **e.** the coordination of DOBDC with Tb(III) leads in the formation of 2-dimensional layered sheets ($\bar{1}01$) which are interlinked by DHBDC to form **f.** the 3-dimensional **SION-1**, with pores along the [010] direction which are occupied by coordinated DMF molecules. Atom colours: orange, Tb; red, O; blue, N; grey, C; pale yellow, H.

Deriving the structural topology of **SION-1** into discrete secondary building units of 1-dimensional Tb-O chains is challenging and has been acknowledged previously for MOFs with similar coordination schemes to 1-dimensional Tb(III)-O chains, such as in MOF-74 analogues.[12, 14] For the topological analysis of **SION-1**, we treated each Tb(III) ion in the 1-dimensional Tb(III)-O chains as a separate node, and using this method ultimately resulting in the net ***lvt*** for **SION-1** (Fig. S6). Here, the DHBDC and

DOBDC ligands are described as connected to four separate Tb(III) nodes. We note that the DOBDC ligands in **SION-1** are coordinated to six Tb(III) ions (Fig. 2d) however, for conceptual symmetry with the ligand binding in **SION-2** we have severed two of these connections in the topological description, corresponding to the terminal carboxylate O-Tb(III) bond on the opposite side of the oxido group.

### Bulk Characterization, Thermal and Chemical Stability of SION-1 and SION-2

The bulk phase and elemental purity of **SION-1** and **SION-2** is confirmed by PXRD, infra-red spectroscopy and elemental analysis, whereas their thermal stability was evaluated by thermogravimetric analysis (SI section S4). Both **SION-1** and **SION-2** are stable standing in air for long periods of time (up to 2 months), however their stability in $H_2O$ is different (Fig. S10 and S11). The PXRD patterns of the $H_2O$ loaded **SION-1@$H_2O$** and **SION-2@$H_2O$** suggested that although they are still crystalline, structural changes have occurred; an observation that was visually confirmed by the change of their colour from gold to beige for **SION-2**, and red to orange for **SION-1**.[15] Both **SION-1@$H_2O$** and **SION-2@$H_2O$** structures were solved using SCXRD, (please see SI sections S2.3-S2.4). We found that **SION-1@$H_2O$** does not undergo substantial structural changes compared to **SION-1**, however, the 3-dimensional structure of **SION-2** collapses into binuclear $Tb_2$-clusters aligned in 1-dimensional chains extended along the $[\bar{1}01]$ direction (Fig. S12 and S13).

## Chemical transformation from SION-2 to SION-1

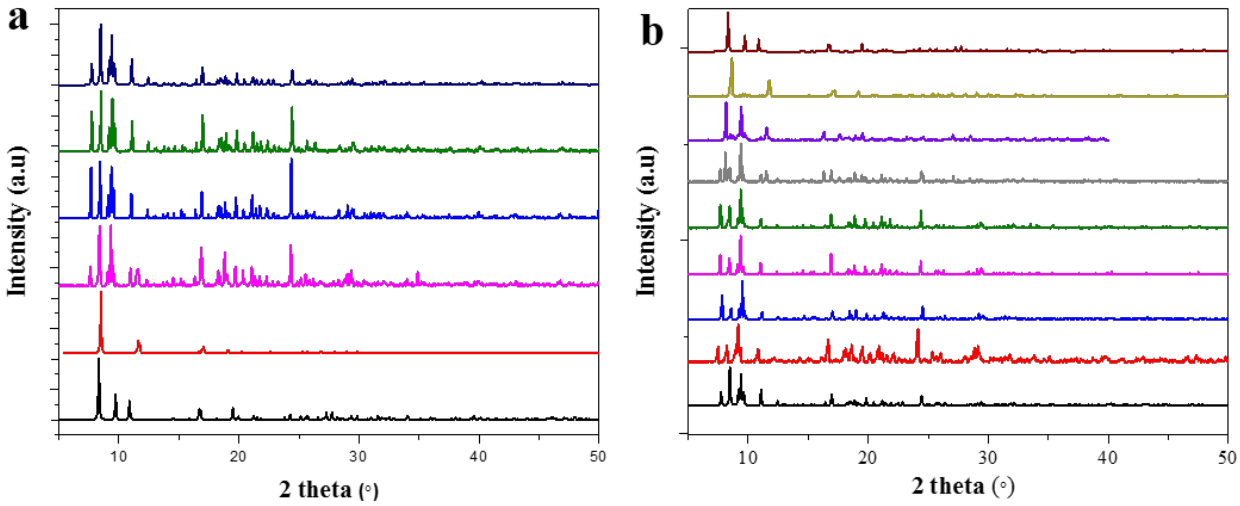


**Fig. 3. a.** Effects of concentration of DMF on the formation of **SION-1** and **SION-2**, here all vials contain 0.5 mL of $H_2O$. Color scheme: black, **SION-1** theory; red, 2.0-2.2 mL DMF; pink, 1.5-1.7 mL DMF; Blue 1.0-1.3 mL DMF; green, **SION-2**; navy blue, **SION-2** theory., **b.** Effects of time on the formation of **SION-1** and **SION-2**. Color scheme: black, **SION-2** theory; red, 12 hrs, blue, 24 hrs; pink, 48 hrs; green, 52 hrs; grey, 62 hrs; purple, 65 hrs; dark yellow, 72 hrs (**SION-1**); brown, **SION-1** theory.

During the screening process, it was observed that both crystals of **SION-2** and **SION-1** could be formed together in the same reaction vial. Therefore, **SION-2** was further examined as an intermediate to **SION-1**, as it forms in shorter times. Preformed **SION-2** was treated using the conditions for the synthesis of **SION-2** and **SION-1**, however the solvent ratio (DMF:$H_2O$) (Fig. 3a) and time (Fig. 3b) was varied. Conditions outside of the optimal DMF:$H_2O$ of 2.0:0.5 mL, time (<12 hrs), and anhydrous DMF led to either no transformation (**SION-2** recovered) or various ratios of the both. Solid state transformation was ruled out through the use of previously air dried **SION 2** crystals, which resulted in no transformation (SI sections S4.6). Therefore, the irreversible Transformation from **SION-2** to **SION-1** only occurs when **SION-2** is submerged in a DMF/$H_2O$ solvent mixture and heated.

## Partial Dissolution of SION-2

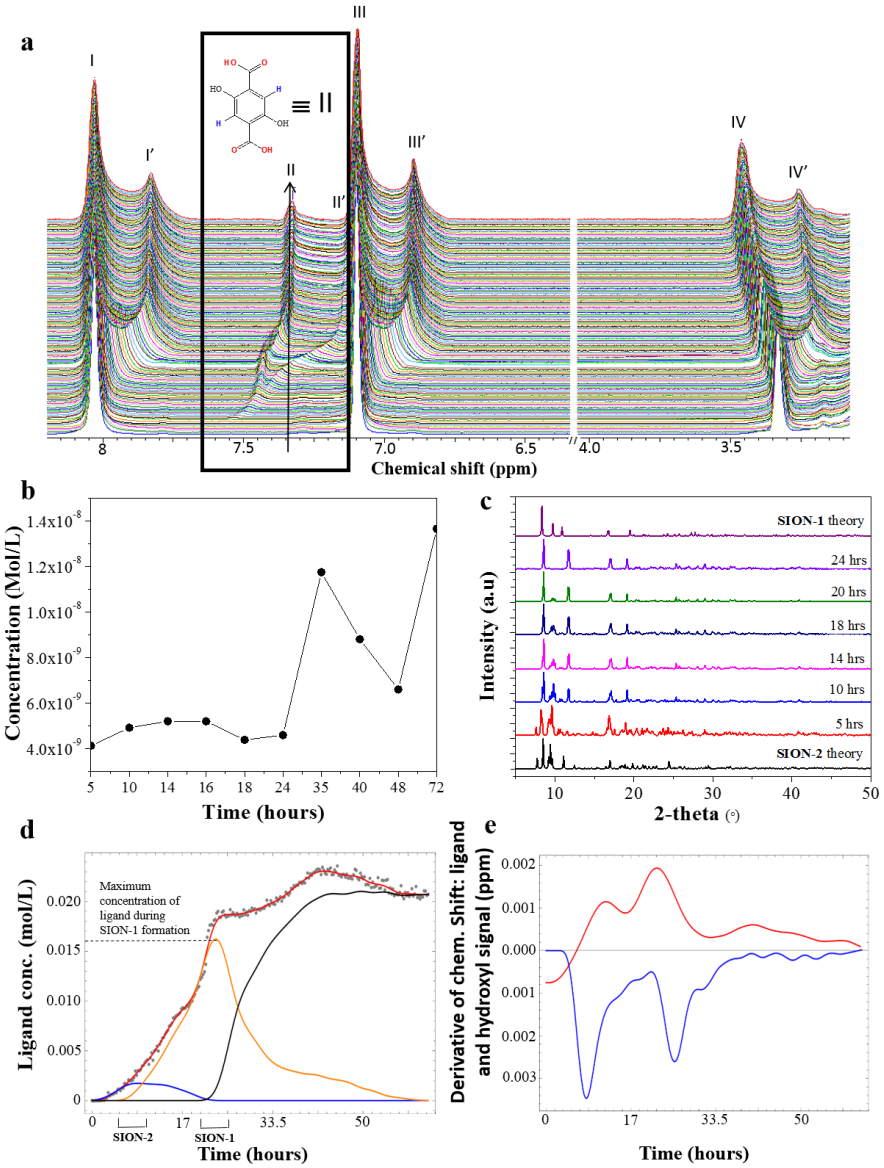


**Fig. 4. a.** Transformation of **SION-2** to **SION-1** observed through $^{1}$H NMR (30-minute interval scans). I-I': $_{d}$-DMF, II-II': DHBDC evolution, III-III': *p*-xylene, IV-IV': $D_2O/H_2O$. **b.** ICP-MS indicating negligible amount of free Tb(III) is released in the liquor during the transformation. **c.** Transformation of **SION-2** to **SION-1** following the changes through PXRD. These times correspond to peaks of the blue and orange lines of Figure d. **d.** Aromatic $^{1}$H DHBDC integral as a function of time. Grey dots: experimental integration determined using Mestre GSD algorithm; red line: is the interpolated function, blue and orange: DHBDC in close proximity to Tb(III), black: free DHBDC. Vertical axis gives the calculated ligand concentration in mol/L based on *p*-xylene integration. **e.** Deviation of chemical shift in the $^{1}$H NMR spectrum of bother the aromatic DHBDC (blue) and hydroxy (red) signals.

Paramagnetism in NMR often leads to difficulty in interpreting spectra due to: *a.* signal broadening through nuclear relaxation from the electronic magnetic moment, and *b.* hyperfine chemical shifts that are dependent on the topological and geometrical locations of each proton with respect to their position from the paramagnetic center.[16] While challenging, structural and electronic information can be revealed through the understanding of these NMR spectra.[16] *In-situ* $^{1}$H NMR experiments were utilized to probe the formation pathway from **SION-2** to **SION-1** by analysing the composition of the $_{d}$-DMF/$D_2O$ solution during heating. Crystals of **SION-2** were immersed in $_{d}$-DMF/$D_2O$ in a sealed NMR tube and heated at 120˚C for 62 hrs (Fig. 4a). After 4.25

hrs we observed the appearance of a peak at 7.60 ppm corresponding to the release of the ligand, followed by a gradual shift to 7.44 ppm (after 12.25 hrs), after which the peak appears to split and continues to shift until reaching 7.33 ppm where it stabilizes (after 38 hrs) for the remaining time. To understand if the cause of the peak splitting is due to the evolution of another DHBDC by-product or a change in the chemical environment of the aromatic H of DHBDC, we have compared the variations in the chemical shift of both DHBDC and OH (from $H_2O/D_2O$) signals; Fig. 4e shows that the changes in both of these occur at approximately the same time, suggesting a simultaneous modification. The release of ligand within the liquor indicates that **SION-2** is partially disassembled and therefore free Tb(III) could be potentially released as the structure rearranges itself. ICP-MS was therefore utilized and confirms the presence of free Tb(III) in extremely low quantities (less than 0.1 % of Tb(III) after 72 hrs) (Fig. 4b). As Tb(III) is paramagnetic, the split of all the peaks in the $^1$H NMR spectrum is attributed to its release. Since the concentration is significantly lower than that of DHBDC, the formation of a molecular complex is ruled out, and instead, we observed a dynamic change from deprotonated DHBDC to protonated $H_2$DHBDC.

Analysis of the $^1$H NMR spectra using the Mestre GSD algorithm reveals the signal of the aromatic proton on the ligand as a function of time, with the ligand concentration determined through the integration of an internal standard (Fig. 4d). The use of ~12 mg of **SION-2** consists of 0.043 mol/L (2.7 x$10^{-5}$ mols, 0.625 mL of solvent used) of DHBDC ligand. Combining the *in-situ* $^1$H NMR for the analysis of the solution media with the PXRD patterns (Fig. 4c), a number of observations have been recorded (Fig. 4d): a. **SION-2** is still present after 5-10 hours of heating but there are traces of ligand leaching into the liquor, b. between 10-20 hours there is a mixture of **SION-1** and **SION-2** and after 24 hours, there is 0.016 mol/L (1.0 x$10^{-5}$ mols) of ligand released corresponding to 37% release of the total ligand (Fig. 4d); c. **SION-1** is formed after a duration of 24 hours, and e. after 24 hours, the ligand released into the solution adopts a new form (protonated $H_2$DHBDC). A release of 37% ligand, represents the loss of approximately 1/3 of the ligands in the $M_2L_3$ (**SION-2**) general formula resulting in $M_2L_2$ (**SION-1**). Therefore, **SION-2** is indeed acting as an intermediate phase for the generation of **SION-1** and the transformation from **SION-2** to **SION-1** occurs through a partial dissolution pathway.

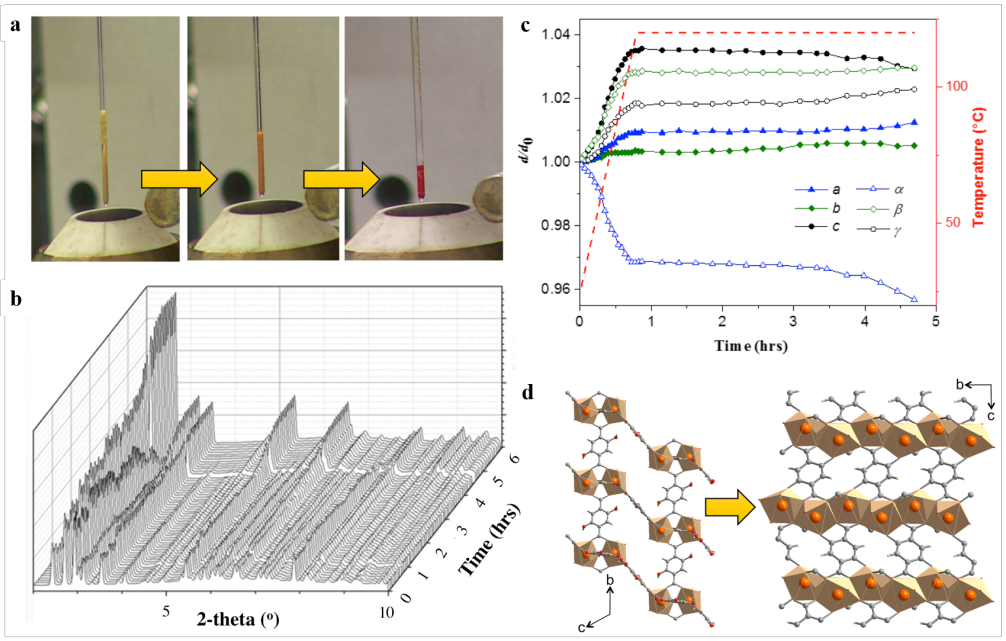


**Fig. 5. a. SION-2** crystalline powder was immersed in DMF:$H_2O$ and packed in a quartz capillary. The reaction was heated at 120 °C for over a period of 6 hrs and as can be seen, the golden color of **SION-2** changed to red upon heating, indicating that **SION-1** is formed. **b.** PXRD patterns collected throughout the reaction evolution. **SION-2** could be fully transformed to **SION-1** within 6 hours. **c.** Temperature dependent evolution of lattice parameters of **SION-2** as a function of time. After 4.7 hours no **SION-2** lattice parameters cannot be longer extracted from

the PXRD data. **d.** General view of the **SION-2** to **SION-1** transformation emphasising the removal of one $\eta^2$-chelating DHBDC ligand (shown in purple) and the re-organisation of $Tb_2$ clusters (shown as pairs of orange spheres along with coordination polyhedra) into Tb–O chains.

The chemical transformation from **SION-2** to **SION-1** was further monitored with an *in-situ* powder X-ray diffraction study (see Section S7). **SION-2** in the form of crystalline powder was immersed in a mixture of DMF:$H_2O$, packed in a quartz capillary and heated at 2 °C $min^{-1}$ to 120 °C, then held at 120 °C for 6 hours, with collection time of 60 secs per PXRD pattern (Fig. 5a-b). Fitting the PXRD data according to the Le Bail method provided us with insights on the evolution of unit cell parameters as a function of temperature and time (Fig. 5c). Anisotropic thermal expansion upon heating to 120 °C is followed by the actual time-dependent transformation. As can be seen in Fig. 5c, the largest magnitude of thermal expansion occurs along the *c*-axis, which suggests a structural instability along the [001] direction of **SION-2** related to the presence of $Tb_2$ dimers and $\eta^2$-chelating DHBDC ligands (as summarised in Fig. 5d, upon the chemical transformation of **SION-2** to **SION-1**, discrete $Tb_2$ clusters reorganise into infinite Tb–O chains, and one out of three DHBDC ligands is removed). Once the temperature of 120 °C is attained, the unit-cell parameters of **SION-2** are stabilised (Fig. 5c), however, after 1.6 hours, we have observed new Bragg reflections evolving which can be indexed with the unit cell of **SION-1**. Subsequently, as the **SION-1** Bragg reflections gain in intensity whereas the diffraction from **SION-2** becomes increasingly weaker and completely disappears after 4.7 hours. There are no additional peaks or amorphous phases present that would indicate the deconstruction of **SION-2** and between 1.6 to 4.7 hours we have observed that the X-ray diffraction patterns consist both phases **SION-1** and **SION-2**. Therefore, the transformation from **SION-2** to **SION-1** occurs without losing crystallinity, and can be followed by the colour change of the samples from gold to red (Fig. 5a).

**Structural Transformation of SION-2 to SION-1.**

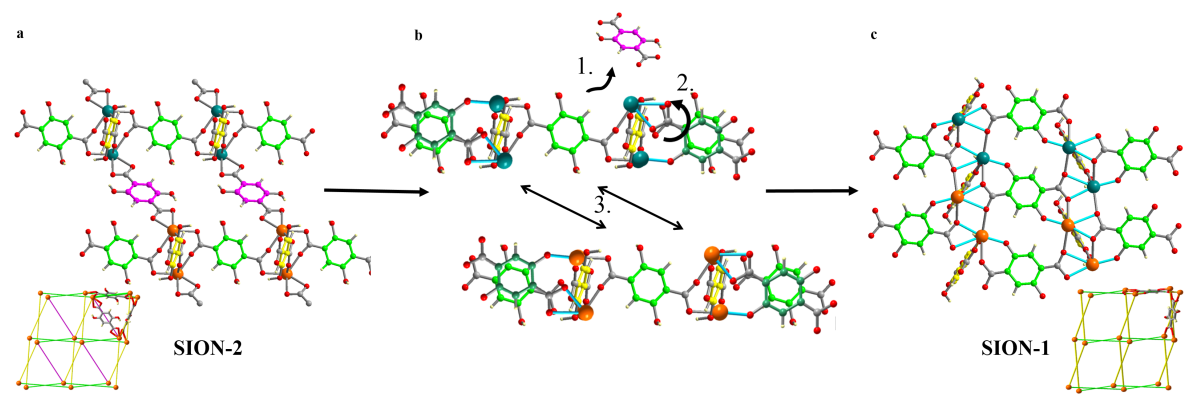


**Fig. 6: a-c.** The chemical transformation from **SION-2** (**a**) to **SION-1** (**c**) through **b1.** partial dissolution of **SION-2** and release of the $\eta^2$-chelating DHBDC ligand (purple), **b2.** rotation of the green DHBDC, and **b3.** shift of the structure leading to the formation of 1-dimensional Tb-O chains upon coordination of the oxido O-atom of DOBDC to the neighboring Tb(III). The transformation can be also rationalized by their network topologies of ***xah*** of **SION-2** (**a**, bottom) and ***lvt*** of **SION-1** (**c**, bottom).

Combining the information gained from the *in-situ* studies with the structural topologies of **SION-2** to **SION-1**, the formation pathway of **SION-1** can be proposed (Fig. 6a-c). The projection of the topologies of **SION-2** along [001] and **SION-1** along [010] shows significant similarities. It is apparent that the ***lvt*** network can be recovered from the ***xah*** by simply eliminating the purple edge, which corresponds to the $\eta^2$- chelating DHBDC ligand. Fig. 6a shows a layer of **SION-2** projected along [010] where the purple DHBDC ligand corresponds to the purple line in the ***xah*** network topology. From this structure, **SION-1** can be formed (Fig. 6c) through the completion of the following steps presented in Fig. 6b. Firstly, the purple $\eta^2$-chelating DHBDC ligand is eliminated, followed by a 180° rotation of the green DHBDC ligands and slight tilt along the [100] direction, which can be achieved by severing one of the Tb-O bonds and, following rotation, forming two new Tb-O bonds, including one with the

oxido group of DOBDC. Finally, the isolated $Tb_2$-clusters, represented in separate layers as dark cyan and orange balls (Fig. 6a-c), join together to form the 1-dimensional Tb-O chains present in **SION-1**. This is achieved by forming new Tb-O bonds with nearby carboxylate O- and oxido O-atoms of the green DOBDC ligands and central (coloured grey and red) ligands, respectively. DFT calculations support this mechanistic hypothesis as the purple $\eta^2$-chelating DHBDC in **SION-2** has a bond energy (-41.347 kcal/mol) which is smaller than the $\eta^1$:$\eta^1$ bridging DHBDC ligands (-59.888 and -65.745 kcal/mol) in **SION-2**, highlighting that their lability is the initial driving force for the transition from **SION-2** to **SION-1** (see Section S8).

## Conclusions

In conclusion, we have observed through multiple analysis that the chemical transformation from the metastable kinetic phase **SION-2** to the stable thermodynamic phase **SION-1** occurs through the partial dissolution of **SION-2.** This is triggered by the loss of the $\eta^2$ chelating DHBDC ligand, followed by internal structural changes resulting in the formation of **SION-1**. To the best of our knowledge, this is the first example of a lanthanide based MOF that is chemically transformed in a solvent mixture, which does not rely on the removal of solvent coordinated to the metal, commonplace for single-crystal to single-crystal transformations occurring under dry conditions.[17] Understanding how MOFs are formed can promote greater control on the assembly of the metal ions or clusters with the ligands and can lead in the identification of stable materials with improved properties compared to the kinetically favoured MOF materials.

## Associated Content

**Supporting Information**. Synthetic protocols, PXRD patterns of all materials reported, IR spectra, TGA profiles and NMR data are shown within the supporting information. The supplementary crystallographic data for this paper were deposited with the Cambridge Crystallographic Data Centre (CCDC) as entries CCDC 1503699-1503702. These data can be obtained free of charge from the CCDC via www.ccdc.cam.ac.uk/data_request/cif.

## Acknowledgements

KCS thanks Swiss National Science Foundation (SNF) for funding under the Ambizione Energy Grant n.PZENP2_166888. BS thanks European Research Council for funding under the European Union's Seventh Framework Programme (FP/2007-2013) / ERC Grant Agreement n.666983 - MaGic. CPI is grateful to the EU for a Marie Curie Fellowship (705861 – ASPAir, H2020-MSCA-IF-2015). The DFT calculations were performed thanks to the access of the Swiss National Supercomputing Center (CSCS) under Project No. s611. SLA and KCS thank Dr S. Bulut and Dr. H. Vrubel for assistance with TGA and ICP-MS experiments respectively. AG, KJG and KCS thank Dr. S. J. Teat and Dr. D. Chernysov for useful crystallography related discussions. The Advanced Light Source is supported by the Director, Office of Science, Office of Basic Energy Sciences, of the U.S. Department of Energy under Contract No. DE-AC02-05CH11231. The authors finally thank ALS (11.3.1) and ESRF (BM01-SNBL) for accessing the single crystal X-ray diffraction beamlines, where the structures of **SION-1@$H_2O$** and **SION-2@$H_2O$** are respectively solved, and the high resolution powder X-ray diffraction beamline BM31-SNBL.

## References

1. (a) Rein ten Wolde, P.; Frenkel, D., *Phys. Chem. Chem. Phys.* **1999,** *1*, 2191-2196; (b) Ostwald, W., *Z. Phys. Chem* **1897,** *22*, 289-330; (c) Cardew, P. T.; Davey, R. J., *Proc. R. Soc. Lond. A* **1985,** *398*, 415-428; (d) Alexander, S.; McTague, J., *Phys. Rev. Lett.* **1978,** *41*, 702-705; (e) Klein, W.; Leyvraz, F., *Phys. Rev. Lett.* **1986,** *57*, 2845-2848; (f) ten Wolde, P. R.; Ruiz-Montero, M. J.; Frenkel, D., *Phys. Rev. Lett.* **1995,** *75*, 2714-2717; (g) Auer, S.; Frenkel, D., *Nature* **2001,** *409*, 1020-1023; (h) Martin, N.; Boruntea, C. R.; Moliner, M.; Corma, A., *Chem. Commun.* **2015,** *51*, 11030-11033.
2. (a) Perić, J.; Vučak, M.; Krstulović, R.; Brečević, L.; Kralj, D., *Thermochimica Acta* **1996,** *277*, 175-186; (b) Ogino, T.; Suzuki, T.; Sawada, K., *Geochim. Cosmochim. Acta.* **1987,** *51*, 2757-2767.
3. Hanaor, D. A. H.; Sorrell, C. C., *J. Mater. Sci.* **2011,** *46*, 855-874.

4. (a) Gándara, F.; de la Peña-O'Shea, V. A.; Illas, F.; Snejko, N.; Proserpio, D. M.; Gutiérrez-Puebla, E.; Monge, M. A., *Inorg. Chem.* **2009,** *48*, 4707-4713; (b) Taouti, M. B.; Suffren, Y.; Leynaud, O.; Benbertal, D.; Brenier, A.; Gautier-Luneau, I., *Inorg. Chem.* **2015,** *54*, 3608-3618; (c) Brozek, C. K.; Michaelis, V. K.; Ong, T.-C.; Bellarosa, L.; López, N.; Griffin, R. G.; Dincă, M., *ACS Cent. Sci.* **2015,** *1*, 252-260.
5. Farha, O. K.; Hupp, J. T., *Acc. Chem. Res.* **2010,** *43*, 1166-1175.
6. Whitelam, S.; Jack, R. L., *Annu. Rev. Phys. Chem.* **2015,** *66*, 143-163.
7. Desgranges, C.; Delhommelle, J., *Phys. Rev. Lett.* **2007,** *98*, 235502.
8. (a) Zhu, N.; Lennox, M. J.; Duren, T.; Schmitt, W., *Chem. Commun.* **2014,** *50*, 4207-4210; (b) Yan, Z.; Li, M.; Gao, H.-L.; Huang, X.-C.; Li, D., *Chem. Commun.* **2012,** *48*, 3960-3962; (c) Frahm, D.; Hoffmann, F.; Fröba, M., *Cryst. Growth Des.* **2014,** *14*, 1719-1725; (d) Morris, R. E., *ChemPhysChem* **2009,** *10*, 327-329; (e) O'Brien, M. G.; Beale, A. M.; Weckhuysen, B. M., *Chem. Soc. Rev.* **2010,** *39*, 4767-4782; (f) Jensen, K. M. Ø.; Tyrsted, C.; Bremholm, M.; Iversen, B. B., *ChemSusChem.* **2014,** *7*, 1594-1611; (g) Goesten, M. G.; Kapteijn, F.; Gascon, J., *CrystEngComm.* **2013,** *15*, 9249-9257.
9. Bellarosa, L.; Brozek, C. K.; García-Melchor, M.; Dincă, M.; López, N., *Chem. Mater.* **2015,** *27*, 3422-3429.
10. (a) Wu, Y.; Breeze, M. I.; Clarkson, G. J.; Millange, F.; O'Hare, D.; Walton, R. I., *Angew. Chem. Int. Ed.* **2016,** *55*, 4992-4996; (b) Yeung, H. H. M.; Wu, Y.; Henke, S.; Cheetham, A. K.; O'Hare, D.; Walton, R. I., *Angew. Chem. Int. Ed.* **2016,** *55*, 2012-2016; (c) Haouas, M.; Volkringer, C.; Loiseau, T.; Férey, G.; Taulelle, F., *Chem. Mater.* **2012,** *24*, 2462-2471.
11. (a) Nayak, S.; Nayek, H. P.; Pietzonka, C.; Novitchi, G.; Dehnen, S., *J. Mol. Struct.* **2011,** *1004*, 82-87; (b) Wang, Y.-L.; Jiang, Y.-L.; Liu, Q.-Y.; Tan, Y.-X.; Wei, J.-J.; Zhang, J., *CrystEngComm.* **2011,** *13*, 4981-4987.
12. Delgado Friedrichs, O.; O'Keeffe, M.; Yaghi, O. M., *Acta Crystallogr. Sect. A* **2003,** *59*, 22-27.
13. Rosi, N. L.; Kim, J.; Eddaoudi, M.; Chen, B.; O'Keeffe, M.; Yaghi, O. M., *J. Am. Chem. Soc.* **2005,** *127*, 1504-1518.
14. O'Keeffe, M.; Yaghi, O. M., *Chem. Rev.* **2012,** *112*, 675-702.
15. Majano, G.; Martin, O.; Hammes, M.; Smeets, S.; Baerlocher, C.; Pérez-Ramírez, J., *Adv. Funct. Mater.* **2014,** *24*, 3855-3865.
16. Piguet, C.; Geraldes, C. F. G. C., Paramagnetic NMR Lanthanide Induced Shifts for Extracting Solution Structures. In *Handbook on the Physics and Chemistry of Rare Earths*, K.A. Gschneidner, J. C. G. B.; Pecharsky, V. K., Eds. Elsevier: 2003; Vol. Volume 33, pp 353-463.
17. (a) Park, I.-H.; Lee, S. S.; Vittal, J. J., *Chem. Eur. J.* **2013,** *19*, 2695-2702; (b) Warren, J. E.; Perkins, C. G.; Jelfs, K. E.; Boldrin, P.; Chater, P. A.; Miller, G. J.; Manning, T. D.; Briggs, M. E.; Stylianou, K. C.; Claridge, J. B.; Rosseinsky, M. J., *Angew. Chem.* **2014,** *126*, 4680-4684.